Multicamera Laparoscopic Imaging With Tunable Focusing Capability

Aditi Kanhere, Kari L. Van Grinsven, Chi-Chieh Huang, Yen-Sheng Lu, Jacob A. Greenberg, Charles P. Heise, Yu Hen Hu, *Fellow, IEEE*, and Hongrui Jiang, *Senior Member, IEEE*

Abstract—**This paper presents a solution to overcome many of the fundamental challenges faced by current laparoscopic imaging systems. Our system is developed upon the key idea that widely spread multiple tunable microcameras can cover a large range of vantage points and field of view (FoV) for intraabdominal visualization. Our design features multiple tunable-focus microcameras integrated with a surgical port to provide panoramic intraabdominal visualization with enhanced depth perception. Our system can be optically tuned to focus on objects within a range of 5 mm to ∞, with a FoV adjustable between 36° and 130°. Our unique approach also eliminates the requirement of an exclusive imaging port and need for navigation of cameras between ports during surgery. [2014-0176]**

Index Terms—**Laparoscopic imaging, tunable focusing, microlens, microcamera array, polarizer.**

I. Introduction

LAPAROSCOPY is a minimally invasive surgical procedure performed through multiple small incisions in the abdomen. These incisions are used to deploy surgical 'trocars' or ports used to introduce cameras and surgical instruments inside a surgical cavity. Current laparoscopic imaging technology relies on a single fixed-focus camera through one of the ports, thus facing five fundamental challenges – limited field of view (FoV), lack of depth perception, occupation of a dedicated port by the camera, need for extensive maneuvering of the camera during surgery by an assistant and glare from highly reflective organ surfaces [1].

A panoramic, 3-dimensional (3D) vision of the surgical field, closely resembling the view in a conventional open surgery, is highly desirable in laparoscopy. It helps expedite surgical tasks and enhances the safety of surgical procedures [2], [3]. A single camera provides a small FoV and limited depth perception due to the flat, 2D view. Some commercial systems claim 3D vision by employing a pair of closely spaced cameras. However, the narrow baseline between the cameras and the resulting low disparity limit the accuracy of depth recovery. More importantly, a two-camera pair cannot provide sufficient viewing angles to ensure an unobstructed view of the surgical region despite the presence of surgical instruments.

In the past, research solutions have proposed using wedge prisms [4], panomorph lenses [5] and mirror attachments [6], [7] to increase the FoV. Nonetheless, these methods suffer from a multitude of issues ranging from aberrations to blind zones. Other research solutions to address these challenges through software techniques for 3-D depth recovery have also had limited success [8].

Current laparoscopes demand one port exclusively for imaging rather than instrumentation. In addition, constant maneuvering of the camera between ports is required to adjust the viewing angle of the surgical field. Several groups have bypassed these requirements by means of imaging tools tethered [9], sutured [10] or magnetically anchored [11] to the abdominal wall. However, these invasive solutions result in additional puncture points or tugging of the abdominal wall, increasing the invasiveness of the laparoscopic procedures.

Other research alternatives such as single-port surgery allowing multiple ports and curved instruments via one site [12] suffer greatly from reduced freedom of movement of surgical instruments and challenging maneuvers, rendering them less practical. Current commercial robotic platforms such as the Da Vinci system [13] offer some advantageous solutions but at the price of very high cost and large footprints.

Existing imaging solutions only address the aforementioned challenges individually and offer partial benefits over the current technology, at best. We previously reported on a reconfigurable fixed-focus, micro-camera array with panoramic vision [14]–[16]. Here we present a new, comprehensive approach to addressing the aforementioned challenges in one system.

II. System Overview

Our system features an integrated trocar-camera assembly (TCA) and a user interface with image acquisition, illumination and optical tuning controls. Our unique approach enables easy adaptability of the system for both single-port and multi-port laparoscopies without compromise on any of the design benefits.

Manuscript received June 6, 2014; revised August 26, 2014; accepted September 21, 2014. Date of publication October 9, 2014; date of current version November 25, 2014. This work was supported by the U.S. National Science Foundation through the Cyber-Physical Systems Program under Grant CNS-1329481, and the Emerging Frontiers in Research and Innovation Program under Grant EFRI-0937847. Subject Editor X. Zhang.

A. Kanhere, K. Van Grinsven, and Y. Hu are with the Department of Electrical and Computer Engineering, University of Wisconsin, Madison, WI 53706 USA (e-mail: kanhere@wisc.edu; kvangrinsven@wisc.edu; hu@engr.wisc.edu).

C.-C. Huang was with the University of Wisconsin, Madison, WI 53706 USA. He is now with Intel Corporation, Oregon, USA. (e-mail: dr.season@gmail.com).

Y.-S. Lu was with the University of Wisconsin, Madison, WI 53706 USA. He is now with Taiwan Semiconductor Manufacturing Company Limited, Taiwan. (e-mail: ysl9527@gmail.com).

J. A. Greenberg and C. P. Heise are with the Department of Surgery, University of Wisconsin School of Medicine and Public Health, Madison, WI 53726 USA (e-mail: greenbergj@surgery.wisc.edu; heise@surgery.wisc.edu).

H. Jiang is with the Department of Electrical and Computer Engineering and the Department of Biomedical Engineering, Materials Science Program, McPherson Eye Research Institute, University of Wisconsin–Madison, Madison, WI 53706 USA (e-mail: hongrui@engr.wisc.edu).

Color versions of one or more of the figures in this paper are available online at http://ieeexplore.ieee.org.

Digital Object Identifier 10.1109/JMEMS.2014.2360124

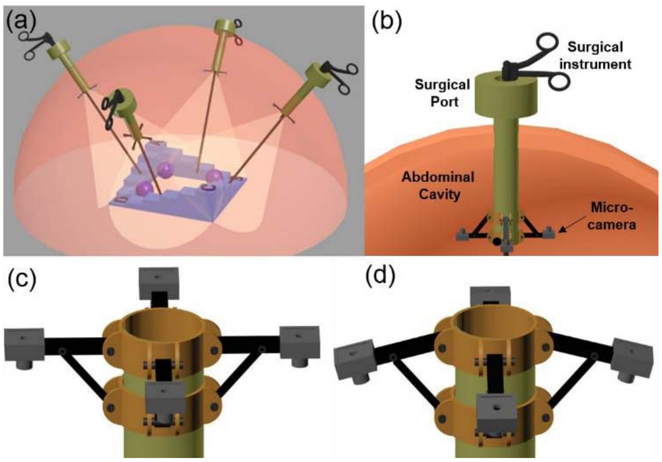

Fig. 1. Schematic representation of (a) our system, as implemented in a multi-port laparoscopic surgery. (b) The cross-sectional view of an integrated trocar-camera assembly after insertion within an abdominal cavity. (c) and (d) The reconfigurability of camera perspectives using an umbrella-like mechanical actuator.

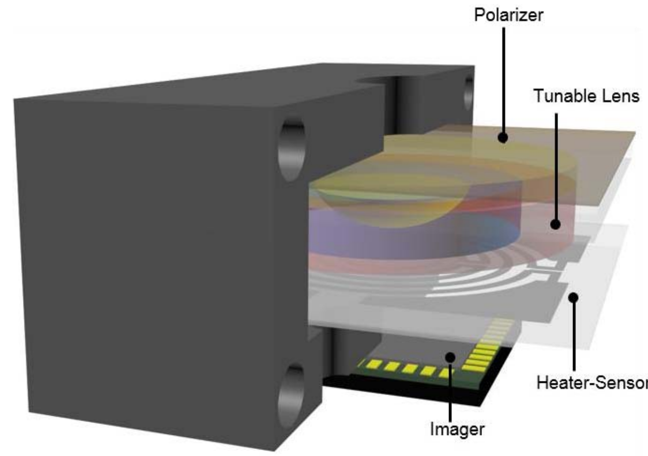

Fig. 2. 3-D representation of the assembly of a microcamera unit. Every camera module comprises of a commercial image sensor (1 mm × 1 mm), a tunable thermo-responsive liquid lens with an integrated heater-sensor and a polarizer.

Fig. 1 shows a schematic of our system, as implemented for multi-port laparoscopy. A hemispherical dome structure is used to illustrate an abdominal, surgical cavity with four incision points or ports. During a laparoscopic procedure, the four TCAs will first be inserted into the surgical cavity, one through each incision (port). Each TCA features an array of four tunable micro-cameras. The TCAs will then be positioned to view the surgical region of interest from four viewing perspectives in such a manner, that most of the scene elements are visible to more than one TCA. The redundancy arising due to such an imaging strategy ensures that every detail in the scene will be captured by at least one port. This feature is critical for viewing smaller elements occluded from view by surgical instruments, shadows or larger elements.

Following this, the images from individual cameras in each TCA will be displayed with focus settings, as controlled by the surgeon and these images can further be combined and processed at his/her wish. There will be no further human intervention required throughout the surgery to move, remove or replace the cameras. The trocar will remain accessible for surgical instruments. The surgeon can acquire images, control the illumination intensity and control the focus of each camera through a user interface panel.

A. Trocar-Camera Assembly

The TCA integrates an array of four microcamera units with a surgical port so that multiple cameras may be deployed into the abdominal cavity through an incision, without any additional surgical operation. In addition, it is affixed to the distal end of the port to capture images, while reconfiguring viewing perspectives through simple mechanical actuation. In our current prototype, the design of the TCA is preliminary, the focus being primarily on assembly and integration of the microcamera units.

The TCA consists of four microcameras assembled symmetrically around the trocar, connected together by a mechanical assembly. The mechanical design of the assembly is similar to an umbrella frame. As shown in Fig. 1(c), the assembly consists of four mechanical arms, each supporting one tunable microcamera. The arms are interconnected via a mechanical assembly that enables opening and closing of the arms, similar to the spokes of an umbrella.

The frame is mounted along the periphery of the distal end of a surgical port, thereby keeping the port accessible. This ensures that the imaging system never interferes with the instruments in the port. The design of the actuation frame enables the reconfiguration of the cameras to ensure complete coverage of the surgical scene without the need for constant maneuvering during surgery.

Images acquired from individual cameras in any one frame position will present distinct yet overlapping viewing perspectives of the same scene. Hence they can be stitched seamlessly for a much wider FoV in the resulting panoramic image. The use of multiple cameras allows for large FoV with reduced aberration (e.g. compared with fisheye-lens) while the optical tunability of the microcameras significantly improves the quality and depth perception of the image.

As shown in Fig. 2, each camera module of the TCA consists of four components – an image sensor, a thermo-responsive tunable lens and an integrated heater-sensor actuator for optical tuning and a polarizer for glare reduction.

B. Variable-Focus Liquid Microlenses

Since the microcameras will be affixed to the port, they must possess tunable focus in order to provide focused images of a surgical scene. Given the dimensions of an abdominal cavity and the positioning of the cameras closer to the abdominal wall, the tuning range of the focal length was designed to range from 5 mm to 50 mm.

The tuning of the focal length was achieved by thermo-responsive hydrogel actuation [17]–[20]. The choice of the tuning mechanism was due to easy, inexpensive fabrication and lack of need for bulky power sources for actuation.

Hydrogel-based tunable lenses have also been shown to have rugged, repeatable performance lasting for about 300

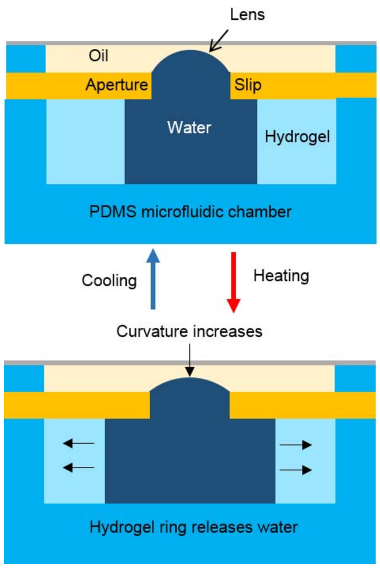

Fig. 3. Schematic representation illustrating the operation of a thermo-responsive tunable liquid lens. As the local temperature increases, the hydrogel releases water and contracts, thereby increasing the radius of curvature and decreasing the focal length of the water-oil lens. This focal length change is reversible.

heating-cooling cycles [20]. The principle of operation of the tunable lenses is represented in the schematic shown in Fig. 3.

The design consists of a thermal stimuli-responsive hydrogel ring placed within a microfluidic chamber filled with water. This chamber is sealed with an aperture slip with a circular opening centered over the ring. An oil chamber is then placed on top of the aperture slip. The opening in the aperture slip acts as the lens aperture. The water-oil meniscus is pinned along the lens aperture by surface treating the layers to create a hydrophobic-hydrophilic contact boundary. The initial meniscus, and thus the focal length, is determined by the volume of water filled in the water chamber. When the temperature of the lens structure is increased, the hydrogel ring responds by contracting due to the release of water via the hydrogel network interstitials. This results in a net change in the volume of the water located in the center of the ring. Since the aperture rim of the lens is pinned, this translates to an increase in the radius of curvature and a decrease in the focal length. This process is reversible with little hysteresis [20], which means that a decrease in temperature will cause the focal length to increase.

C. Integrated Microheater-Sensor

The factors influencing our choice of the microheater were (1) form factor suitable for easy integration with lenses, (2) uniformity of heat distribution, (3) ease of heat dissipation after operation and (4) preventing thermal shock to the image sensor. We chose a coil type resistive heater design for easy alignment with the hydrogel ring structure. The coil design also minimizes hotspots due to absence of sharp corners [21].

D. Polarizer

The presence of bodily fluids in the body makes the internal organ surfaces highly reflective, resulting in a glare while imaging them [22]. Glossy or highly reflecting surfaces often reflect a linearly polarized component of the incoming light much more strongly than the others. Therefore, our approach to addressing this challenge was to integrate a polarizer in front of our tunable-focus lens. We fabricated a linear polarizer oriented so as to block the reflected linear component. Such selective transmission of incident light based on the plane of polarization enhances the contrast of objects against the background, especially in low light conditions such as a surgical cavity.

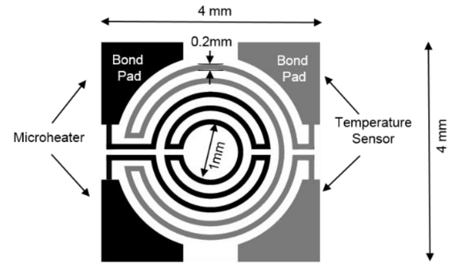

Fig. 4. Schematic of the integrated microheater-sensor design. The coil track shown in black is the microheater; whereas the coil shown in gray the temperature sensor. The width of the coil track is 0.2 mm whereas its thickness is 200 nm.

III. Design Considerations

A. Tunable Microlenses

An important design consideration during fabrication of tunable lenses is the Lower Solution Critical Temperature (LCST) of the hydrogel. The LCST is the temperature point where a sharp phase transition occurs in the hydrogel. When heated to temperature above the LCST, the hydrogel responds by rapidly releasing water or contracting, thus reducing the focal length. When the temperature changes from above the LCST to below the LCST, the hydrogel volume changes by a factor of 10 [23]. During a surgery, it is undesirable to have an uncontrolled change in the focal length of a camera. Normal human body temperature is about 37 °C. If the LCST of the hydrogel is close to 37 °C, the focal length of the lens will change in response to body heat. To avoid this, we set the LCST of the hydrogel at 42 °C, to account for the deviations in body temperatures of patients.

The second important factor to be considered in tunable lens design is the focal length. Laparoscopic surgeries are most commonly performed within the abdominal cavity. Typically, a laparoscopic imaging system should be capable of viewing small features at the far end of the surgical cavity as well as the larger protrusions, closer to the port. Hence we designed our liquid lenses with capability to tune within a wide range of 5 mm to 50 mm. The two main factors determining the focal length range of our tunable lenses are the lens aperture diameter and the actuation temperature. The lens aperture diameter of 1 mm was constrained by the smallest available commercial image sensor – 1 mm × 1 mm NanEye cameras (AWAIBA Lda, Madeira, Portugal). The constraint on the temperature is placed by the higher temperature resistance limit of our commercial image sensor ($T_{max} = 90$ °C).

B. Integrated Microheater-Sensor

Ideally the change in the focal length of the microlens should closely track the actuation temperature of the microheater. To this end, we chose the coil type design of the microheater to align directly under the hydrogel ring pattern. In addition, the microheater was encapsulated inside the sensor coil, as shown in Fig. 4, so as to ensure accurate sensing and feedback control. The heating material should be made of a material with a high thermal conductivity to ensure a short response time. We chose aluminum (Al) as the heater material for ease of fabrication.

Since the microheater is resistive, its resistance will change with temperature and can be calculated from the equation

$$R_t = R(1 + \alpha T)$$

R_t – Resistance at temperature, T

R – Resistance at ambient temperature, 25 °C

α – Temperature coefficient of resistance (0.00429 for Al at 25 °C).

Resistance of the microheater at ambient temperature of 25 °C can be calculated from the equation

$$R = \frac{\rho L}{wt}$$

ρ – Resistivity(2.82×10^{-8} Ω-m for Al at 25 °C)

L – Length of heater

w – width of heater

t – thickness of heater.

For our microheater dimensions (L = 28.634 mm; w = 0.1 mm; t = 250 nm), its resistance at room temperature is 32.29 Ω.

IV. Fabrication Methods

The tunable lenses were fabricated using liquid-phase photopolymerisation (LP^3) [17]–[20]. The thermo-responsive hydrogel, N-isopropylacrylamide (NIPAAm) was used to actuate the tunable lenses. The intrinsic LCST of NIPAAm is 32 °C. It was adjusted to 42 °C by incorporating 0.15 percent by volume of an ionizable monomer, 3-(methacryloylamino) propyl trimethylammonium chloride (MAPTAC), into NIPAAm.

A 300 μm thick cavity was defined on a glass substrate using double-sided adhesive spacers. This cavity was filled with a poly(isobornyl acrylate) (IBA) prepolymer mixture. Poly-IBA posts defining the water container (Ø = 2.5 mm) were photopatterned through a photomask aligned on top of the cavity under UV radiance (8.0 mW cm^{-2} for 75 s). The chamber was then rinsed with ethanol to remove the unexposed solution. Another 200 μm thick chamber was created on top of this structure to define the base of the water container. Then the chamber was filled with pre-cured polydimethylsiloxane (PDMS) and cured at 70 °C for 8 h, before being peeled off the poly-IBA mold. The sidewalls of the PDMS water containers were treated to be hydrophilic by corona discharge plasma. The water containers were then filled then with the NIPAAm (with added MAPTAC) hydrogel pre-polymer solution and then were photopatterned under UV radiance (I = 15 mW cm^{-2}; t = 18 s) to form hydrogel rings in the containers.

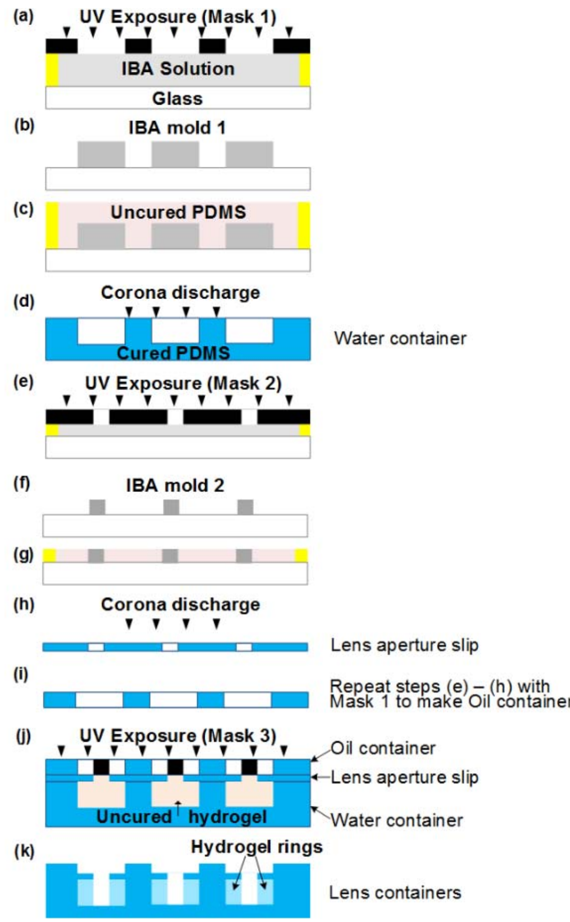

Fig. 5. Fabrication process flow for thermo-responsive hydrogel based tunable liquid lenses. (a-d) Cylindrical water containers (Ø = 2.5 mm) were defined in polyIBA molds and then transferred onto PDMS. The top surface of the PDMS containers was rendered hydrophilic by corona discharge. (e-h) Similar processes were carried out to define the lens aperture slip (Ø = 1 mm) and (i) oil containers (Ø = 2.5 mm). (j-k) The three layers were bonded together. The water containers were then filled with NIPAAm hydrogel and photopatterened to form hydrogel rings

Similar procedures were carried out to form a 250 μm thick PDMS with 1 mm circular openings defining the lens aperture. The side walls of the aperture were surface treated to be hydrophilic so as to form a pinning boundary for the water-oil lens. Then another 250 μm thick PDMS layer with a 2.5 mm aperture was bonded on top of the aperture slip to form the oil container. The containers were filled with deionized water and silicon oil consecutively, forming the immiscible water–oil interfaces for the microlenses. The cross section of this fabrication process is shown in Fig. 5.

Thermal actuation and tuning of the lens was achieved with a microheater placed at the base of the lens, fabricated as shown in Fig. 6 using lift-off process. A layer of PDMS was first spun onto a photoresist coated glass slide and cured at 70 °C for 4 hours. Subsequently, a 2 μm thick layer of Parylene-C was deposited onto the PDMS layer, to improve the adhesion of metal onto PDMS. A 250 nm thick Al layer

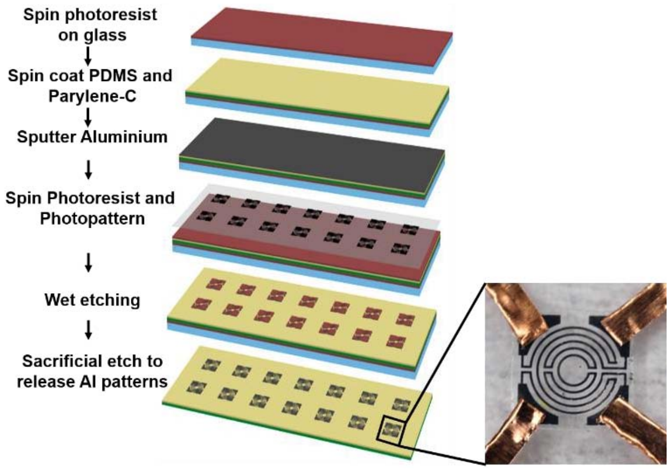

Fig. 6. Fabrication process flow for aluminum micro heater coil patterned on PDMS using lift-off process.

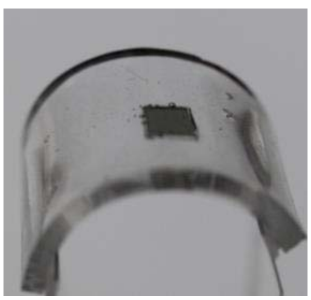

Fig. 7. Image of a thin film Polyvinyl Alcohol (PVA) polarizer patterned on a flexible PDMS substrate.

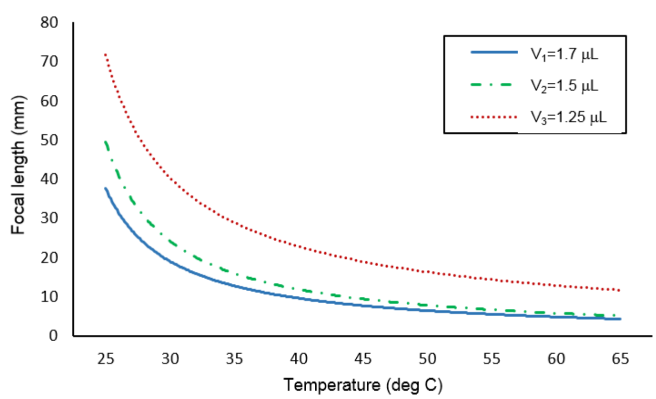

Fig. 8. Focal lengths of microlenses plotted against temperatures for initial water volumes of 1.25 μL, 1.5 μL, and 1.7 μL filled in the liquid lenses. 1.5 μL water containers yielded an optimum focal length range when the temperature was varied from 42 °C to 75 °C.

was then sputtered onto this layer followed by photolithography and wet etching (H_3PO_4:HNO_3:CH_3COOH:H_2O in ratio 3:3:1:1 at 40 °C for 75 s) to define the microheater coil.

A thin film PVA polarizer, shown in Fig. 7 was fabricated on a flexible substrate and integrated in front of the camera. A cleaned glass substrate surface was first mechanically etched to pre-define the orientation of the subsequently made polarizing film. A pre-polymer of doped Polyvinyl Alcohol (PVA) was then spin-coated on at 1500 rpm for 1 minute onto the

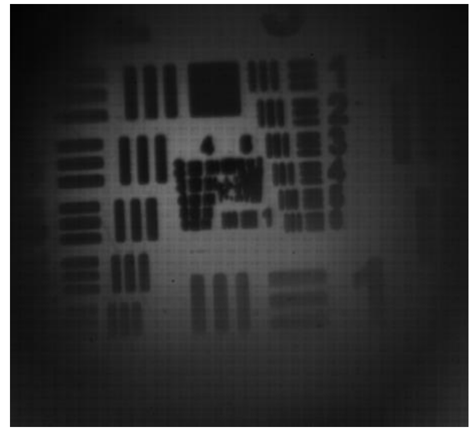

Fig. 9. Image of the 1951 USAF resolution target as seen by a microlens with a focal length of 20 mm. The smallest resolvable features are element 3 in group 3 corresponding to a resolution of 10.10 line pairs/mm.

glass substrate (thickness $\sim$ 500 μm). The surface was heated at 100 °C for 20 minutes to evaporate the solvent and cure the PVA thinfilm. The PVA thinfilm was subsequently peeled off the glass substrate. A PDMS elastomer was then mixed with a curing agent in 10:1 ratio by weight. The mixture was then placed in the vacuum chamber to extract air bubbles. It was then poured onto two glass slides, cured at 80 °C for 4 hours and then peeled off to yield two flexible PDMS films (thickness $\sim$ 250 μm). The PVA thinfilm was then sandwiched and bonded between the two thin PDMS films to yield the flexible linear polarizer film.

V. User Interface

A graphical user interface was designed using the LabVIEW (National Instruments Inc., Austin, TX, USA.) programming environment, to provide unified controls for focus tuning, image acquisition and illumination controls. The heater, sensor and the light source were monitored and controlled using the CompactDAQ chassis cDAQ-9172 in conjunction with the analog input module, NI 9201 and the output module, NI 9264. A closed-loop temperature control was implemented for the integrated heater-sensor device. The image acquisition and visualization from the cameras was done directly via the sensor USB board.

VI. Results and Discussion

A. Focal Length Measurements

For identical temperatures, the focal length range of microlenses varies with the initial volume of water filled in the water containers. To analyze these variations, three sets of microlenses were fabricated with initial water volumes of 1.25 μL, 1.5 μL, and 1.7 μL. Within each set were five microlenses with the same initial water volume. The focal lengths of these microlenses were measured by computing the distance at which a collimated laser light passing through the microlens can be focused onto an optical screen. Fig. 8 shows a plot of the focal lengths versus temperature, averaged for each water volume. The average response time to tune a

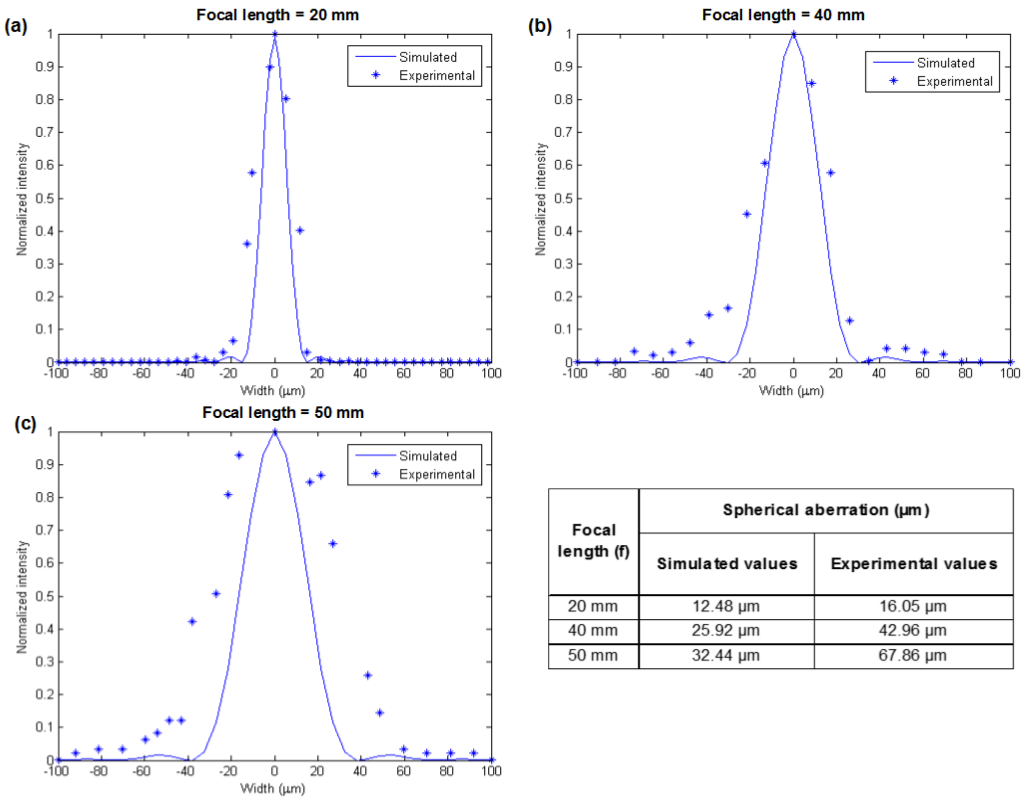

Focal length (f)	Spherical aberration (μm)	
	Simulated values	Experimental values
20 mm	12.48 μm	16.05 μm
40 mm	25.92 μm	42.96 μm
50 mm	32.44 μm	67.86 μm

Fig. 10. Simulated and experimental normalized light intensity profiles obtained by imaging a laser beam focused by microlenses at focal lengths (a) 20 mm (b) 40 mm and (c) 50 mm. The corresponding spherical aberration values shown in the table are calculated as the full width at half maximum.

lens between the two extremes of its focal length range was ~20 seconds.

Across the temperature range of 42 °C to 70 °C, an initial water volume of 1.5 μL yields a focal length range suitable for our application. For all the subsequent experiments, the initial water volume filled in the microlenses was 1.5 μL. However, even with the same initial water volume, the focal length of different lenses at the same temperatures varies within an error margin of 10%. This is due to the variations in the temperature-dependent volume change of hydrogel rings.

B. Imaging Performance of Tunable Lens

The resolving power of the lens was measured by imaging a 1951 USAF resolution test chart. Fig. 9 shows the image obtained by a microlens tuned to a focal length of 20 mm. The smallest resolvable features were 10.10 line pairs per mm.

The lens design was simulated using the sequential ray tracing mode of a commercial light-ray tracing software, ZEMAX (ZEMAX Development Corporation, Bellevue, WA, USA). The pinned water-oil interface was assumed to be spherical since the two liquids have comparable densities [24]. Point spread function (PSF) analysis was performed to yield normalized light intensities at three different focal lengths.

Spherical aberrations at these focal lengths were then calculated as the full width at half maximum of the PSF [20], as shown in Fig. 10. The normalized light intensity profiles at different focal lengths, and the corresponding spherical aberrations were also measured experimentally. A collimated laser source (632 nm) was used to illuminate a tunable microlens from the bottom. The image of the focused laser spot was recorded using a CCD camera (BCN-C050-U, Mightex Systems, Toronto, ON, Canada). As the focal length of the lens was tuned, the camera was moved along the optical axis and positioned at the focal point. Normalized light intensities were extracted from these images at three different focal lengths and the corresponding spherical aberrations were calculated. Fig. 10 shows that the experimental and simulation results for spherical lens aberrations are in agreement within a reasonable margin of error.

C. Microheater-Sensor Characterization

The thermal behavior of the microheater design was analyzed using ANSYS simulation software (ANSYS, Inc.). The heat dissipation from the heater to the surrounding air (T = 25 °C) was assumed to be through convection. The steady state thermal-electric analysis module of ANSYS was employed to simulate the temperature distribution in the heater. The results in Fig. 11 show that the heat distribution is localized within the heating element.

Also, the temperature towards the edges of the device is much lower. This is crucial in our design to avoid over-heating of the surrounding tissue, since this could pose a high risk during surgery [25]. Within the active heater region, temperature uniformity is obtained within a reasonable tolerance 6.66%. The results in Fig. 11 were simulated at a time step of t = 1 s, indicating a very rapid ramp up to the desired temperature in the heating element.

To calibrate the heater and the sensor, each of their resistances was measured against the reference temperature of a

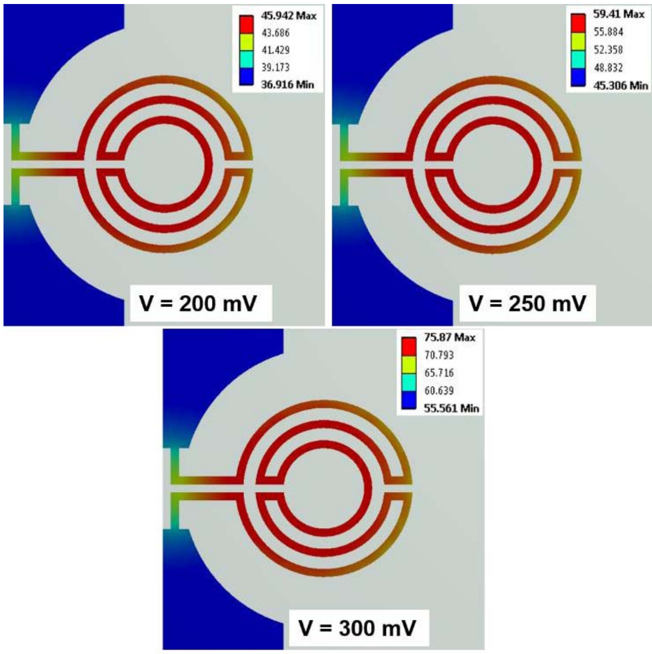

Fig. 11. Simulation results for temperature of the microheater at time $t = 1$ s for actuation voltages of 200 mV, 250 mV and 300 mV. The heat is localized and uniformly distributed in the heating element within a tolerance of 6.66%.

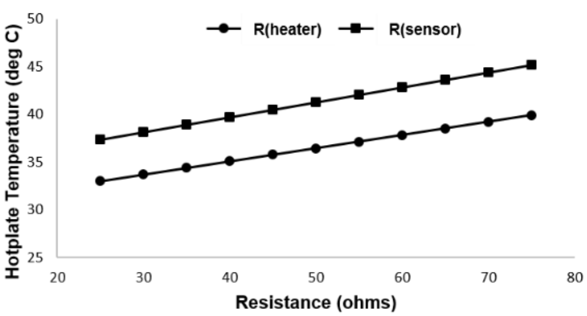

Fig. 12. Calibration curves for heater and sensor resistances.

hot plate. The resistances were noted for set points between 20 °C and 75 °C during both - heating and cooling cycles. The solid lines in Fig. 12 indicate the fitting curves to account for hysteresis between heating and cooling cycles. This is the calibration plot used for the feedback control of the temperature of the microheater.

D. Polarizer

To test the selective transmission of incident light when passed through the polarizer, we passed a linearly polarized HeNe laser beam ($\lambda = 630$ nm) through the polarizer. The polarizer was rotated to vary the angle of the incident polarization with respect to the polarizer. It can be seen from Fig. 13 that maximum light is transmitted when the incident light is aligned in the same direction as the polarizer and polarization perpendicular to the polarizer orientation is completely blocked.

E. Imaging

The effects of integration of a polarizer in front of the camera while imaging reflective surfaces were tested by placing a highly reflective metal nail in the center of the scene

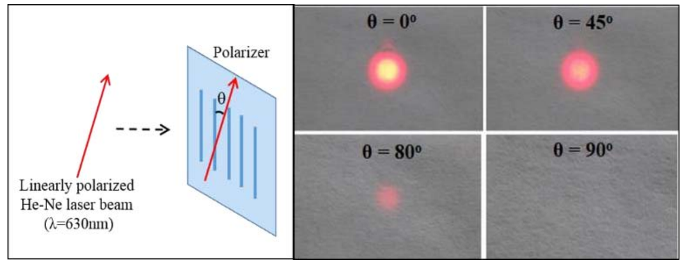

Fig. 13. Selective transmission of a linearly polarized He-Ne laser ($\lambda = 630$ nm) when passed through the polarizer.

Fig. 14. Reduction in glare with the use of a polarizer as seen from comparison of an image without using a polarizer in front of a tunable camera (left) and the same image captured with a polarizer in front of the lens (right).

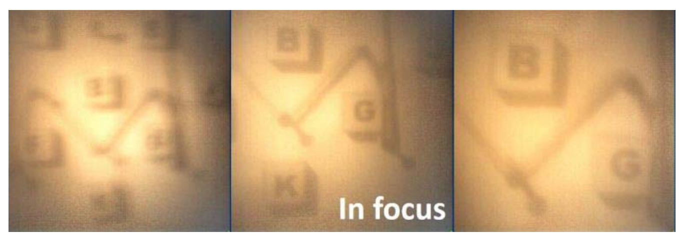

Fig. 15. Images of a test scene as captured by a single camera while the focal length of its tunable liquid lens was being tuned using a microheater.

being imaged. Fig. 14 demonstrates effective glare reduction while imaging with the use of a polarizer.

To test the optical focusing capabilities of our cameras, the position of a single tunable camera was fixed 12 cm away from the test scene. The test scene comprised of a periodic arrangement of 9 dice (1.5 cm × 1.5 cm × 1.5 cm) forming a rhombus (length = 16 cm). Images of the scene were then captured by the camera while varying the temperature from 45 °C to 65 °C to tune the lens. Fig. 15 shows a series of three images captured by a camera while tuning the thermo-responsive lens using a microheater. The scene is first out of focus; then the camera gradually focuses in on the scene as the lens is tuned.

Commercial laparoscopic trainer boxes are often used to develop laparoscopic skills, using inanimate tasks, in novice surgeons. A common training task assignment is to stretch a rubber band around nails tacked on a board [26]. We modeled our test surgical scene to closely mimic this training setup, as shown in Fig. 16(e). The test scene was placed in a dark environment with illumination provided solely with a fiber optic light guide to closely resemble a surgical cavity. Since the NanEye image sensors do not have an IR filter, an

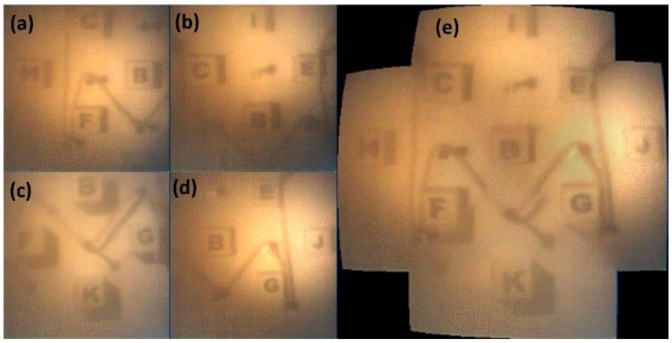

Fig. 16. Images of a mimicked surgical scene as captured by our camera array. (a)–(d) Sharp images of all the sub scenes were obtained by individual cameras. These scenes were then stitched together in a commercial software, PTGui^{TM} to obtain a very large field of view compared to any single camera alone (e).

IR cut was placed at 680 nm to filter the incident light for faithful color imaging.

To test the implementation of our imaging setup in the mock surgical scene, the test scene was sealed within a box with a small opening, similar to an incision in a surgical cavity. The TCA assembly was introduced into the scene along with a fiber optic light guide for illumination. During insertion, the mechanical arms (with the microcameras) were in a closed configuration with the arms parallel to the sidewalls of the port. Once the surgical port was positioned, the arms of the frame were flared out. Initially, the orientation angle of the array was adjusted to provide the desired viewing perspective, depth of field and horizontal field of view. Finer adjustments were then made to ensure distinct but slightly overlapping sub-scenes, as seen by individual cameras. In our design, the orientation angle of all the microcameras can be simultaneously adjusted within an error margin of 5°.

First, the camera lenses were tuned individually to obtain focused images of each of their sub-scenes. This independent optical tuning feature enables our imaging system to handle different object distances without affecting the overall depth perception of the scene. So sharp images of all the sub scenes are obtained by individual cameras as seen in Fig. 16(a-d). These scenes were then stitched together in a commercial software PTGui^{TM} to obtain a panoramic image shown in Fig. 16(e). As seen from the figure, this yields to enhanced depth perception and a significantly large field of view of 128°, which is greater than that of any of the individual source images.

All the images in Fig. 14–16 are unprocessed, raw images. that suffer from low brightness levels, as shown in the histogram in Fig. 17(a). However even some preliminary post processing of the intensity levels of the histogram can significantly improve image quality, as seen in Fig. 17(b) and (c).

The vignetting seen around the edges in individual camera images can be attributed to variation in illumination intensity with change in camera orientation. Also, image distortion can be observed in the panorama in Fig. 16(e) that is not seen in any of the sub-scene source images. However, this is primarily due to limitations of the commercial software.

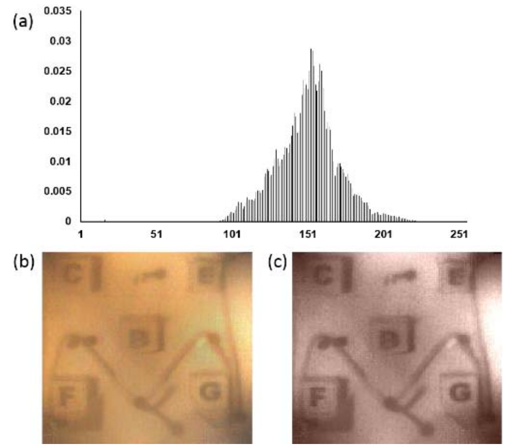

Fig. 17. (a) Pixel intensity distribution (histogram) of the panoramic image in Fig. 16(e). (b) Cropped panoramic image before processing. (c) Cropped panoramic image after redistribution of the intensity levels in the histogram.

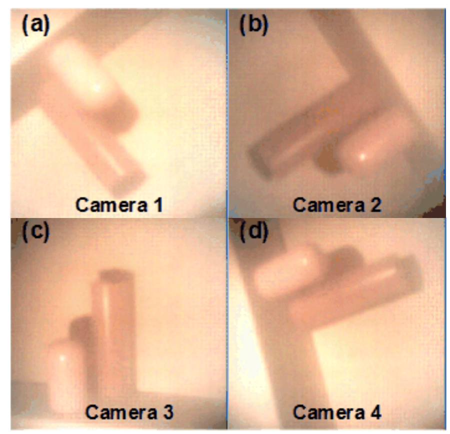

Fig. 18. Enhanced depth perception due to multi-camera array. (a-d) Images of two tubes (Ø = 15 mm) separated by a distance of 10 mm, as captured by four cameras in the TCA. Imaging the same object with a multi-camera array yields depth cues from four different viewing perspectives, leading to an enhanced depth perception compared to any single camera alone.

To demonstrate the enhancement in depth perception with the multi-camera array, we imaged a scene with two tubes placed one behind the other, separated by a distance of 10 mm. The scene was imaged with all four cameras of the TCA at an arbitrary orientation angle. As can be seen in Fig. 18, while imaging the scene with a single camera, the depth-wise separation of different objects may (Fig. 18(c) and (d)) or may not (Fig. 18(a) and (b)) be apparent. However, while imaging with our multi-camera array, the same scene can be viewed from four different viewing perspectives thus leading to increased information about the relative positions of the two objects.

VII. Conclusion

In summary, we demonstrated a tunable, multi-camera laparoscopic imaging system. Our system directly integrates multiple tunable microcameras with the surgical ports. Preliminary results presented in this paper demonstrate panoramic, large-FoV visualization with enhanced depth perception of the surgical cavity by stitching views from multiple microcameras.

A graphical user interface was also developed to enable the surgeons to focus in and out of different features of the surgical scene and control the illumination within the surgical cavity. The integrated trocar-camera assembly offers the surgeon a less-interruptive imaging solution without the need for dedicated imaging ports or inter-port camera navigation during surgery. Our unique approach thus provides promising solutions to several challenges faced by current laparoscopic imaging systems.

Future work will focus on optimization of lens design with emphasis on improving resolution and contrast. Mechanical redesign to integrate an illumination source with each camera will be geared towards minimizing defects like vignetting. Other work will involve development of an image-stitching algorithm optimized for performance in low-light environments as well as customized post-processing techniques for faithful reproduction of the scene. Our future goals also include wireless data transfer, algorithm development for 3D reconstruction, unified user interface design and commercial-grade packaging.

Acknowledgment

The authors would like to thank Dr. B. Aldalali for technical discussion and assistance, and Computer Aided Engineering, University of Wisconsin, Madison, for access to ANSYS 14.5.

References

[1] H. Xin, J. S. Zelek, and H. Carnahan, "Laparoscopic surgery, perceptual limitations and force: A review," in *Proc. 1st Can. Student Conf. Biomed. Comput.*, vol. 144. Kingston, ON, Canada, 2006, pp. 44–49.

[2] Y. Naya *et al.*, "Usefulness of panoramic views for novice surgeons doing retroperitoneal laparoscopic nephrectomy," *Int. J. Urol.*, vol. 16, no. 2, pp. 177–80, 2008.

[3] S. B. Bhayani and G. L. Andriole, "Three-dimensional (3D) vision: Does it improve laparoscopic skills? An assessment of a 3D head-mounted visualization system," *Rev. Urol.*, vol. 7, no. 4, pp. 211–214, 2005.

[4] E. Kobayashi, K. Masamune, I. Sakuma, and T. Dohi, "A wide-angle view endoscope system using wedge prisms," in *Medical Image Computing and Computer-Assisted Intervention*. Berlin, Germany: Springer-Verlag, 2000, pp. 661–668.

[5] P. Roulet, P. Konen, M. Villegas, S. Thibault, and P. Garneau, "360° endoscopy using panomorph lens technology," *Proc. SPIE*, vol. 7558, pp. 1–13, Feb. 2010.

[6] R. Sagawa *et al.*, "Omnidirectional vision attachment for medical endoscopes," in *Proc. 8th Workshop Omnidirectional Vis., Camera Netw. Non-Classical Cameras*, Marseille, France, 2008.

[7] N. Arber, R. Grinshpon, J. Pfeffer, L. Maor, S. Bar-Meir, and D. Rex, "Proof-of-concept study of the Aer-O-Scope omnidirectional colonoscopic viewing system in ex vivo and in vivo porcine models," *Endoscopy*, vol. 39, no. 5, pp. 412–417, 2007.

[8] D. Stoyanov, A. Darzi, and G. Z. Yang, "A practical approach towards accurate dense 3D depth recovery for robotic laparoscopic surgery," *Comput.-Aided Surgery*, vol. 10, no. 4, pp. 199–208, 2005.

[9] C. A. Castro *et al.*, "A wireless robot for networked laparoscopy," *IEEE Trans. Biomed. Eng.*, vol. 60, no. 4, pp. 930–936, Apr. 2013.

[10] T. Hu, P. K. Allen, T. Nadkarni, N. J. Hogle, and D. L. Fowler, "Insertable stereoscopic 3D surgical imaging device with pan and tilt," in *Proc. 2nd IEEE RAS EMBS Int. Conf. Biomed. Robot. Biomechatron.*, Scottsdale, AZ, USA, Oct. 2008, pp. 311–316.

[11] S. L. Best and J. A. Cadeddu, "Development of magnetic anchoring and guidance systems for minimally invasive surgery," *Indian J. Urol.*, vol. 26, no. 3, pp. 418–422, 2010.

[12] L. Mereu, S. Angioni, G. B. Melis, and L. Mencaglia, "Single access laparoscopy for adnexal pathologies using a novel reusable port and curved instruments," *Int. J. Gynaecol. Obstetrics*, vol. 109, no. 1, pp. 78–80, 2010.

[13] R. M. Satava, J. C. Bowersox, M. Mack, and T. M. Krummel, "Robotic surgery: State of the art and future trends," *Contemp. Surgery*, vol. 57, pp. 489–499, Oct. 2001.

[14] A. Kanhere, B. Aldalali, J. A. Greenberg, C. P. Heise, L. Zhang, and H. Jiang, "Reconfigurable micro-camera array with panoramic vision for surgical imaging," *J. Microelectromech. Syst.*, vol. 22, no. 5, pp. 989–991, Oct. 2013.

[15] A. Kanhere *et al.*, "Multi-camera laparoscopic imaging with tunable focusing capability," in *Proc. Solid-State Sens., Actuators, Microsyst. Workshop*, Hilton Head Island, SC, USA, Jun. 2014, pp. 379–382.

[16] B. Aldalali, J. Fernandes, Y. Almoallem, and H. Jiang, "Flexible miniaturized camera array inspired by natural visual systems," *J. Microelectromech. Syst.*, vol. 22, no. 6, pp. 1254–1256, 2013.

[17] L. Dong, A. K. Agarwal, D. J. Beebe, and H. Jiang, "Adaptive liquid microlenses activated by stimuli-responsive hydrogels," *Nature*, vol. 442, pp. 551–554, Aug. 2006.

[18] L. Dong, A. K. Agarwal, D. J. Beebe, and H. Jiang, "Variable-focus liquid microlenses and microlens arrays actuated by thermoresponsive hydrogels," *Adv. Mater.*, vol. 19, no. 3, pp. 401–405, 2007.

[19] D. Zhu, C.-W. Lo, C. Li, and H. Jiang, "Hydrogel-based tunable-focus liquid microlens array with fast response time," *J. Microelectromech. Syst.*, vol. 21, no. 5, pp. 1146–1155, 2012.

[20] X. Zeng, C. Li, D. Zhu, H. Cho, and H. Jiang, "Tunable microlens arrays actuated by various thermo-responsive hydrogel structures," *J. Micromech. Microeng.*, vol. 20, no. 11, p. 115035, 2010.

[21] C. F. Chau and T. Melvin, "Design and fabrication of a quasi-ordered nanoporous silicon membrane suitable for thermally induced drug release," *J. Micromech. Microeng.*, vol. 22, no. 8, p. 085028, 2012.

[22] E. W. Abel, Y. Zhuo, P. D. Ross, and P. S. White, "Automatic glare removal in endoscopic imaging," *Surgical Endoscopy*, vol. 28, no. 2, pp. 584–591, 2014.

[23] J. Wang *et al.*, "Self-actuated, thermo-responsive hydrogel valves for lab on a chip," *Biomed. Microdevices*, vol. 7, no. 4, pp. 313–322, 2005.

[24] S. Kuiper and B. H. W. Hendriks, "Variable-focus liquid lens for miniature cameras," *Appl. Phys. Lett.*, vol. 85, no. 7, pp. 1128–30, Aug. 2004.

[25] R. Lu, S. Liu, X. Luo, and B. Zhang, "Thermal safety analysis of capsule endoscope," in *Proc. 7th ICEPT*, Aug. 2006, pp. 1–4.

[26] E. Hiemstra, W. Kolkman, M. A. van de Put, and F. W. Jansen, "Retention of basic laparoscopic skills after a structured training program," *Gynecological Surgery*, vol. 6, no. 3, pp. 229–235, 2009.

Aditi Kanhere received the B.S. degree in electronics and telecommunication engineering from the University of Pune, Pune, India, in 2009, and the M.S. degree in electrical engineering from the University of Wisconsin–Madison, Madison, WI, USA, in 2011, where she is currently pursuing the Ph.D. degree with the Department of Electrical Engineering. Her research focuses on development of improved surgical imaging tools. Her other research interests include optical MEMS, tunable optics, and low-light imaging.

Kari L. Van Grinsven received the B.S. degree in applied physics from Rice University, Houston, TX, USA, in 2013. At Rice University, she conducted research in a variety of topics, including modeling of photon-positron collisions, ultracold atoms, and microcoil NMR. She is currently pursuing the Ph.D. degree with the Department of Electrical and Computer Engineering, University of Wisconsin–Madison, Madison, WI, USA, and is also a 3M Fellow under sponsorship of the 3M Foundation. Her research interests include optical MEMS devices, novel form factor cameras, and optical cyber physical systems.

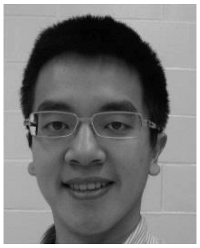

Chi-Chieh Huang received the B.S. degree in materials science and engineering from National Tsing-Hua University, Hsinchu, Taiwan, R.O.C., in 2006, and the M.S. degree in electrical engineering from National Chiao-Tung University, Hsinchu, Taiwan, R.O.C., in 2008. After serving in the Air Force as a second Lieutenant in Taiwan, he was with the Advanced Device Platform for 28-nm CMOS technology at Taiwan Semiconductor Manufacturing CorpCompany, Ltd., Hsinchu, as a Research Device and Process Integration Engineer, from 2009 to 2010. He received the Ph.D. degree in electrical engineering from the University of Wisconsin–Madison, Madison, WI, USA, in 2014. He is currently with Intel Corporation, Santa Clara, CA, USA, as a Senior PTD (Portland Technology Development) Module and Integration Device Yield Engineer. His research interests consist of nanoelectronics device physics and nanofabrication technology, biophotonics, and flexible electronics.

Yen-Sheng Lu received the B.S. degree in mechanical engineering from National Chiao Tung University, Hsinchu, Taiwan, in 2003; the M.S. degree from the Department of Nanoengineering and Microsystems, National Tsing Hua University, Hsinchu, in 2005; and the Ph.D. degree from the Institute of Electronics Engineering, National Tsing Hua University, in 2009. From 2011 to 2012, he was a Visiting Scholar in Mechanical Engineering with the Massachusetts Institute of Technology, Cambridge, MA, USA, and he joined the Department of Electrical and Computer Engineering, University of Wisconsin–Madison, Madison, WI, USA, as a Post-Doctoral Researcher, in 2013. His research interests include optofluidics, liquid lens, and the fundamental study of III-nitride semiconductors, III-nitride-based ambient sensors, and nanofabrication. He is currently with Taiwan Semiconductor Manufacturing Company, Ltd., Hsinchu, where he is involved in developing 20-nm process technology.

Jacob A. Greenberg received the M.D. degree from the University of Pennsylvania School Of Medicine, Philadelphia, PA, USA, and completed his General Surgery Residency at Brigham and Women's Hospital, Boston, MA, USA. During his Residency, he received the Master's degree in education from the Harvard Graduate School of Education, Cambridge, MA. He completed a fellowship in minimally invasive and bariatric surgery at the University of Massachusetts Memorial Medical Center, Worcester, MA. He is currently an Assistant Professor of Surgery with the University of Wisconsin School of Medicine and Public Health, Madison, WI, USA. He is certified by the American Board of Surgery, and he specializes in the minimally invasive treatment of obesity, benign esophageal and gastric conditions, and abdominal wall hernias. His research interests include surgical education and treatment of abdominal wall defects.

Charles P. Heise received the M.D. degree from the University of Minnesota Medical School, Minneapolis, MN, USA, and completed his General Surgery Residency at the University of Wisconsin Hospital and Clinics, Madison, WI, USA, and a Fellowship in colon and rectal surgery at the University of Minnesota, Minneapolis. He is currently a Professor with the Division of General Surgery, Department of Surgery, University of Wisconsin School of Medicine and Public Health, Madison, where he also serves as the Director of Surgical Operations. He is certified by the American Board of Colon and Rectal Surgery and the American Board of Surgery. His specialties include the surgical treatment of colorectal cancer and inflammatory bowel disease. He performs laparoscopic bowel surgery for benign and malignant diseases. His research interests include treatment of diverticulitis, and patient outcome and function after surgical treatment of colorectal cancer and inflammatory bowel disease.

Yu Hen Hu (M'83–SM'88–F'99) received the B.S.E.E. degree from National Taiwan University, Taipei, Taiwan, in 1976, and the M.S.E.E. and Ph.D. degrees from the University of Southern California, Los Angeles, CA, USA, in 1982. He was with the faculty of the Department of Electrical Engineering with Southern Methodist University, Dallas, TX, USA. Since 1987, he has been with the Department of Electrical and Computer Engineering, University of Wisconsin–Madison, Madison, WI, USA, where he is currently a Professor. In 1999, he was a Visiting Researcher with Bell Laboratories, Homedel, NJ, USA, and Microsoft Research–China, Beijing, China. In 2007, he was a Visiting Scholar with the Institute of Electronics, National Taiwan University, and a Visiting Professor with Chung Hwa University, Hsinchu, Taiwan.

He has broad research interests ranging from design and implementation of signal processing algorithms, computer-aided design and physical design of very large scale integration, pattern classification and machine learning algorithms, and image and signal processing in general. He has authored over 300 technical papers, and edited and co-authored three books and many book chapters in these areas.

Dr. Hu has served as an Associate Editor of the IEEE TRANSACTIONS OF ACOUSTIC, SPEECH, AND SIGNAL PROCESSING; the IEEE SIGNAL PROCESSING LETTERS; the *European Journal of Applied Signal Processing*; the *Journal of VLSI Signal Processing*; and the IEEE MULTIMEDIA MAGAZINE. He has served as the Secretary and an Executive Committee Member of the IEEE Signal Processing Society, a Board of Governor of the IEEE Neural Network Council representing the Signal Processing Society, and the Chair of the Signal Processing Society's Neural Network for Signal Processing Technical Committee and the IEEE Signal Processing Society's Multimedia Signal Processing Technical Committee. He was also a Steering Committee Member of the International Conference of Multimedia and Expo on behalf of the IEEE Signal Processing Society.

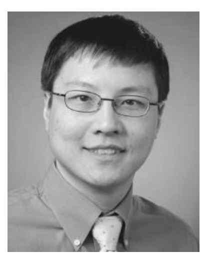

Hongrui Jiang (S'98–M'02–SM'10) received the B.S. degree in physics from Peking University, Beijing, China, and the M.S. and Ph.D. degrees in electrical engineering from Cornell University, Ithaca, NY, USA, in 1999 and 2001, respectively.

He was a Post-Doctoral Researcher with the Berkeley Sensor and Actuator Center, University of California at Berkeley, Berkeley, CA, USA, from 2001 to 2002. He is currently the Vilas Distinguished Achievement Professor and Lynn H. Matthias Professor of Engineering with the Department of Electrical and Computer Engineering, a Faculty Affiliate with the Department of Biomedical Engineering, a Faculty Member of the Materials Science Program, and a Member of the McPherson Eye Research Institute, University of Wisconsin–Madison, Madison, WI, USA. He is a currently an Editorial Board Member of the IEEE JOURNAL OF MICROELECTROMECHANICAL SYSTEMS. His research interests are in microfabrication technology, biological and chemical microsensors, microactuators, optical microelectromechanical systems, smart materials and micro/nanostructures, lab-on-a-chip, and biomimetics and bioinspiration.

Dr. Jiang was a recipient of the National Science Foundation CAREER Award and the Defense Advanced Research Projects Agency Young Faculty Award in 2008, the H. I. Romnes Faculty Fellowship of the University of Wisconsin–Madison in 2011, the National Institutes of Health Director's New Innovator Award in 2011, and the Vilas Associate Award of the University of Wisconsin–Madison in 2013.